Materials & Design 212 (2021) 110287

Contents lists available at ScienceDirect

Materials & Design

journal homepage: www.elsevier.com/locate/matdes

Effect of organic resin in glass wool waste and curing temperature on the synthesis and properties of alkali-activated pastes

Patrick N. Lemougna [a,b], Adeolu Adediran [a], Juho Yliniemi [a], Tero Luukkonen [a], Mirja Illikainen [a]

[a] Faculty of Technology, Fibre and Particle Engineering Research Unit, PO Box 4300, 90014 University of Oulu, Oulu, Finland
[b] Department of Materials and Chemistry, Vrije Universiteit Brussel, Pleinlaan 2, 1050 Brussels, Belgium

HIGHLIGHTS

- The resin in glass wool waste could be gradually eliminated by thermal treatment from 200 to 550 °C.
- The resin affected the milling efficiency, rheology, heat of reaction and strength development.
- Curing at 40 °C was beneficial for strength development in comparison to 20 and 60 °C.
- The 28-days compressive strength was less affected by the presence of the resin.
- The incorporation of suitable co-binders would increase the materials' stability.

GRAPHICAL ABSTRACT

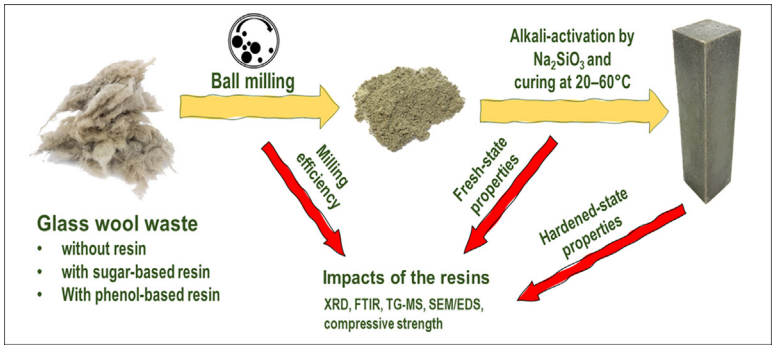

ARTICLE INFO

Article history:
Received 25 July 2021
Revised 25 November 2021
Accepted 26 November 2021
Available online 27 November 2021

Keywords:
Glass wool
Organic resin
Curing temperature
Alkali-activated materials
Mechanical properties
Building applications

ABSTRACT

This study investigated the effect of organic resin contained in glass wool on synthesis of alkali-activated binders. The study was performed on glass wool containing sugar or phenolic resin, comparing it with glass wool that did not contain resin, as a reference. The results showed that the organic resin could be qualitatively identified using Fourier-transform infrared spectroscopy (FTIR) and thermo gravimetry-mass spectrometer (TG-MS), with gradual decomposition occurring between 200 °C and 550 °C. The presence of organic resin reduced the milling efficiency of glass wool, modified the rheology by increasing the liquid demand, and slowed the strength development at room temperature. However, interestingly, the effect of the resin on the strength of the paste was less obvious at an age of 28 days. Curing for 24 h at 40 °C was beneficial for one-day strength development, in comparison to 20 °C and 60 °C, independent of the presence of the resin. All the cured paste samples, with and without resin, achieved a compressive strength of more than 40 MPa at 28 days, satisfying the requirement for many structural applications. Nevertheless, water immersion affected the materials' strength, suggesting their suitability for dry environments or the need for suitable co-binders to increase their durability and water resistance.

1. Introduction

Mineral wool is a common insulating material used in construction [1,2]. It includes glass wool and stone wool, respectively representing about one-third and two-thirds of the volume produced

E-mail addresses: lemougna@yahoo.f, Patrick.ninla.lemougna@vub.be (P.N. Lemougna), Juho.Yliniemi@oulu.fi (J. Yliniemi), tero.luukkonen@oulu.fi (T. Luukkonen)

https://doi.org/10.1016/j.matdes.2021.110287
0264-1275/

[3]. The production and use of mineral wool generate waste; while the production of mineral wool results in dust, construction and demolition activities often produce end-of-life mineral wool and offcut pieces [3,4]. Most glass wool wastes—estimated at a weight of about 800,000 tons per year at the European level [4]—are still landfilled, increasing the socioeconomic concerns related to mineral wool producers and to construction and demolition activities [3]. To date, only a limited number of studies are available on the reuse of glass wool wastes [4–6], despite their similarity with many waste glasses that have been substantially studied. Indeed, glass wool and many waste glasses are X-ray amorphous, with SiO_2, Na_2O, and CaO being the main oxide components [4,5,7–10]. The potential reuse options for glass wastes reported in the literature have included supplementary materials for cements and concretes [10,11], geopolymers or alkali-activated materials [12,13], as well as raw materials and fluxing agents for ceramics [14–19].

Considering the similarities between many glass wastes, the small number of studies and reports on upcycling glass wool could be due to its fibrous structure and the presence of organic resin in glass wool. However, it was recently demonstrated that this fibrous structure could be destroyed by appropriate milling, facilitating the reuse of glass wool waste as a secondary raw material [20]. Amongst the possible valorization routes, geopolymers—or alkali-activated building materials— appear to be a promising option, due to the mild temperatures involved in the process, the simplicity of the preparation process, and the interesting properties of the prepared materials [3,5,21–23].

However, most studies on alkali-activated glass wool have been performed on materials collected from glass wool production lines, before the addition of the organic resin, to prevent any possible interference from the resin on the results. Indeed, glass wool often contains about 5 to 10 wt% of organic resin to facilitate the compaction operation. Based on information collected from glass wool manufacturers, the two most common types of organic resin are phenolic binder and sugar-based binder, also known by its tradename, "green binder." Green binder is formed by the polycondensation of naturally occurring plant-based components—that are, monosugars with an organic acid—while phenolic binder is formed by a polymerization reaction between phenol, formaldehyde, and urea.

Few studies were found in the literature on the alkali activation of glass wool containing resin [3,24–26]. Li et al. [24] worked on improving the reactivity of glass wool containing resin by blending it with slag and mixing it with an alkaline solution. The co-activation of glass wool and slag enhanced the reactivity and the properties of the paste samples at room temperature. Pavlin et al. [26] investigated the effect of the curing regime, activator concentration, and liquid-to-solid ratio used in glass wool and stone wool containing organic binder and observed better mechanical properties in glass wool containing organic binders; such materials achieved a strength of 58 MPa at room temperature. However, there is still a knowledge gap about the role of different types of resin during the alkali activation of glass wools, even though a large proportion of the glass wool waste that needs to be recycled contains organic resin.

The present study investigated the influence of two types of organic resin on the properties of glass wool waste, as well as on the synthesis and properties of resulting alkali-activated materials. Three types of glass wool were used: the reference glass wool without the resin (GW-r), the glass wool containing sugar resin (GW-s), and the glass wool containing phenolic resin (GW-p). The three glass wools were first characterized using thermogravimetric analysis and differential scanning calorimetry (TG/DSC), coupled with mass spectroscopy (MS). The parameters studied during the preparation of the alkali-activated materials from the three different wools included the milling efficiency, rheology, curing temperature (20 °C, 40 °C, and 60 °C), and heat of the reaction. X-ray diffraction (XRD), Fourier-transform infrared spectroscopy (FTIR), scanning electron microscopy coupled with energy dispersive X-ray spectroscopy (SEM-EDS), and compressive test were also used to characterize the glass wools and resulting alkali-activated materials.

2. Methodology

2.1. Materials

The GW-s and GW-p used in this study were provided in a premilled state by the company ISOVER, located in Billesholm, Sweden, while the GW-r (i.e., with no organic resin) was provided by Saint-Gobain Finland Oy in Helsinki, Finland. Despite the premilling of both the GW-s and GW-p, the fibers still appeared to be intact, similar to the GW-r (later shown in Fig. 7). Accordingly, the as-received glass wools were ground in a tumbling ball mill (Germatec, Germany) to reduce the particle size. The milling was performed at 82 rpm using a 10 L jar with 150 balls (45 balls of ϕ40 mm, 45 balls of ϕ 30 mm, and 60 balls of ϕ 25 mm). In total, 300 g of as-received glass wools was loaded into the ball mill container for each milling batch. The milling time was first fixed at one hour for all the wools but was then adjusted to 1 h 20 min and 1 h 30 min for the GW-p and GW-s, respectively, resulting in approximately the same particle size distribution for the three wools. The particle size distribution of every batch of milled glass wool was determined by a laser diffraction particle size analyzer (Beckman Coulter LS 13320, USA), using the Fraunhofer model. Isopropanol was used as the dispersion liquid to ensure the proper dispersion of the wool particles during particle size measurement.

The as-received glass wools were analyzed with X-ray fluorescence (XRF), using an Omnian AxiosmAX (Malvern Panalytical, UK). The chemical composition obtained by XRF revealed that the major oxides present in all the glass wools studied were SiO_2, Na_2O, and CaO, together with other minor oxides (Table 1). The difference shown in Table 1 between the loss on ignition (LOI) at 105 °C and that at 525 °C can be ascribed to the presence of organic resin in the GW-s and GW-p. In addition to the oxide compositions shown in Table 1, glass wool contains about 4 wt% B_2O_3, which could not be quantified using the XRF technique that was applied in this study [5].

The alkaline solution used for the synthesis was a commercial-grade sodium silicate (Betol 52 T, Woellner, Germany) made of 14.7 wt% Na_2O, 30.3 wt% SiO_2 and 55 wt% H_2O.

2.2. Sample preparation

The alkaline solution used for the synthesis was prepared by diluting the commercial-grade sodium silicate with 10 wt% demineralized water. The solution was then stored in a sealed plastic bottle for 24 h at room temperature before use. The dilution was done to reduce the alkalinity of the silicate solution and to improve the workability of the paste. The molar ratio of the activating solution was SiO_2/Na_2O = 2.5. The precursors and the alkali activator were first stirred and mixed for 3 min at 1000 rpm using an electric mixer (IKA EUROSTAR, Germany). Then, the walls of the container were scraped for 1 min and mixed again for 3 min. The amount of activating solution used was adjusted to obtain approximately the same consistency among the pastes prepared with the different wools because they presented a different liquid demand. However, the same solution (same concentration and pH) was used for the 3 glass wools. The mixed paste samples were cast into oiled 20 × 20 × 80 mm^3 steel molds, according to a modified EN 196–

Table 1
Chemical composition in wt% of the GW-r, GW-s, and GW-p.

Samples	SiO_2	Al_2O_3	Fe_2O_3	CaO	MgO	Na_2O	K_2O	TiO_2	P_2O_5	SO_3	Cl	LOI 105 °C	LOI 525 °C
GW-r	63.3	1.5	0.5	8.2	3.1	16.5	0.5	0.0	0.2	0.2	0.1	0	0.06
GW-s	63.5	1.6	0.4	8.4	1.8	17.1	0.6	0.1	0.5	0.1	0.1	0.4	8.1
GW-p	63.8	1.6	0.5	8.4	1.8	16.9	0.5	0.1	0.2	0.7	0.1	0.5	7.4

1 standard [27] and compacted using a jolting machine to remove any trapped air. The details of the mix design are presented in Table 2.

Three curing regimes were employed for the 28-day curing period: (1) room temperature for 28 days; (2) 40 °C on the first day, followed by room temperature for 27 days; and (3) 60 °C on the first day, followed by room temperature for 27 days. All the prepared samples were unmolded after the first day and remained at room temperature (approximately 23 ± 2 °C) until the testing time.

2.3. Calorimetry and rheology analysis

The cumulative heat released from the alkali-activated paste samples of the three glass wools was studied using a TAM Air isothermal calorimetry instrument (TA Instruments, USA), at 20 °C, 40 °C, and 60 °C, during the first 24 h of the reaction. The samples were mixed ex-situ, and a constant A/P of 0.75 was maintained for the 3 types of glass wool studied. Samples with A/P as in table 2 were also prepared and measured for comparison.

Table 2
Mixture proportions.

Ref.	GW-r (g)	GW-s (g)	GW-p (g)	Liquid alkali activator (g)	Activator-to-precursor ratio (A/P)
A_GW-r	100	0	0	50	0.50
A_GW-s	0	100	0	53	0.53
A_GW-p	0	0	100	70	0.70

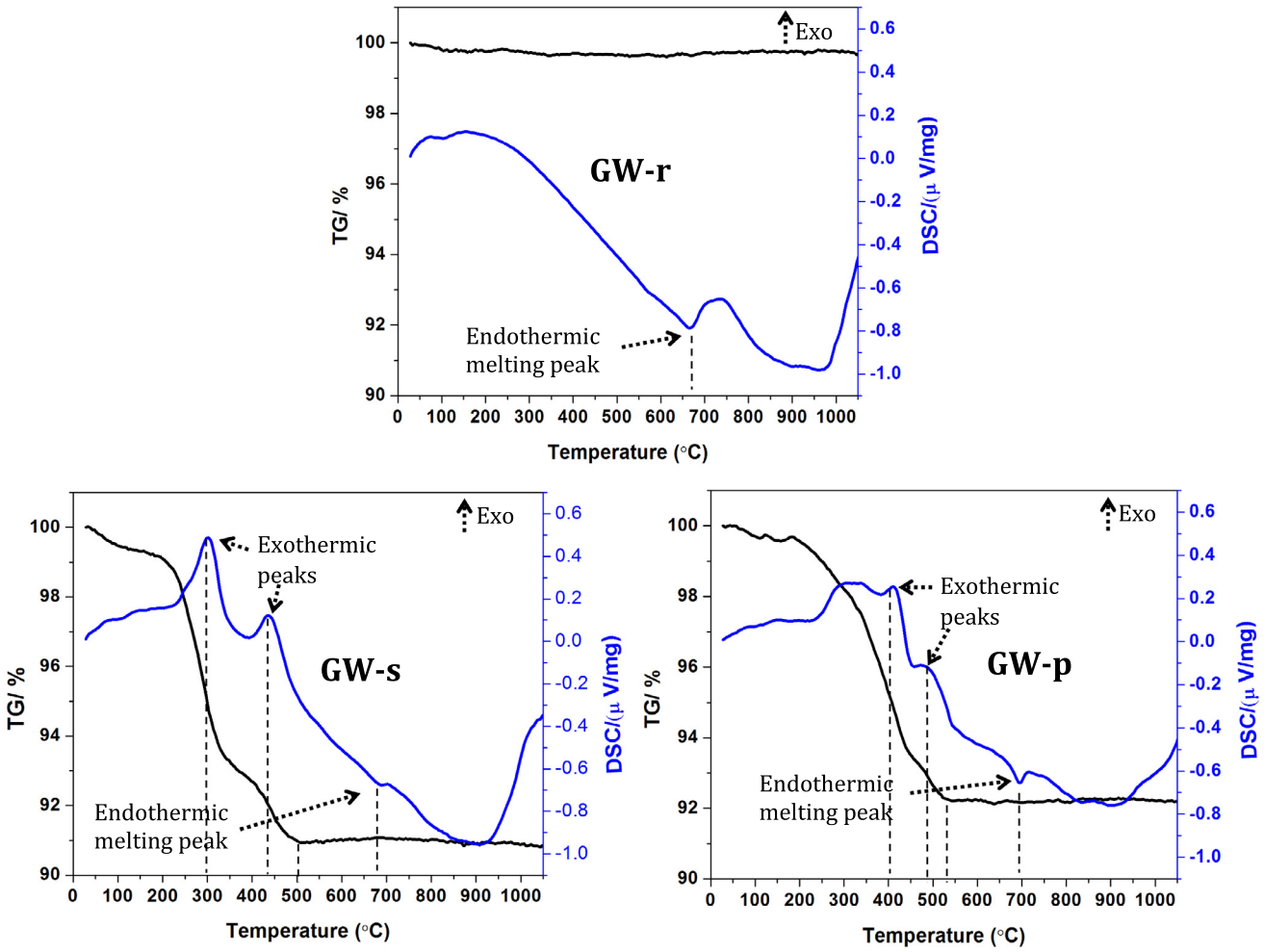

Fig. 1. TG/DSC curves of GW-r, GW-s, and GW-p.

For the rheology study, the A/P was adjusted to 0.8 for the 3 wools, to reach a suitable flowability in the rheometer device. The rheology test (i.e., the measurement of the shear stress versus shear rate) was performed at 20 °C using a Discovery HR-1 rheometer (TA Instruments, USA).

2.4. Characterization methods

2.4.1. TG/DSC-MS analysis

TG/DSC coupled with MS was performed on the samples using a NETZSCH device (Germany). The samples were heated to 1000 °C at 5 °C/min in air, and the released gas was analyzed using a mass spectrometer, in the mass-to-charge ratio (m/z) range of up to 100.

2.4.1. FTIR analysis

The glass wool and resulting alkali-activated materials (at an age of 28 days) were examined by FTIR analysis using a Bruker VERTEX 80 FT-IR spectrometer (USA). The spectra were collected within the range of 4000 cm^{-1} to 400 cm^{-1} using a resolution of 2 cm^{-1}.

2.4.2. SEM/EDS analysis

Fractured pieces of prepared alkali-activated materials were analyzed using SEM-EDS (Zeiss Ultra Plus device, Germany). The surface of the samples was coated with carbon prior to analysis. Analyses were performed with a secondary electron detector with an acceleration voltage of 15 kV, and the working distance was about 8 mm.

2.4.3. XRD analysis

The prepared alkali-activated materials were ground into powder and examined by XRD using a Rigaku SmartLab diffractometer (USA), with Cu K-beta radiation, a step width of 0.02°, a scan speed of 4.0628° per min, a 2θ range of 5° to 80°, and a 20 mm receiving slit. The diffractometer was operated at 135 mA and 40 kV.

2.4.4. Compressive strength and water stability test

A ZwickRoell (Austria) universal testing machine with a maximum load of 100 kN was used for the compressive strength test. The strength measurement was carried out according to the standard EN 196–1:2016; but instead of the prismatic beams with dimensions of 40 × 40 × 160 mm^3, half-sized beams with dimensions of 20 × 20 × 80 mm^3 were used. The prismatic beams were halved for compressive strength assessment. A steel plate with dimensions of 20 × 20 mm^2 was placed on top of the half-specimen before measurement. The measurement was conducted using 2.4 kN/s loading rate. At least three replicated specimens were tested for each composition, and the average was considered as the representative value. The error bars in the strength values (Fig. 11) indicated the standard deviation between the measurements. The compressive strength was determined using the following equation:

$$CS = F/A \quad (1)$$

where CS is the compressive strength in N/mm^2, F is the load or force in N, and A is the cross-sectional area in mm^2.

The stability in water of the prepared alkali-activated materials was also evaluated, including the wet and wet–dry strength (i.e., the strength after immersing the specimens in water for 24 h

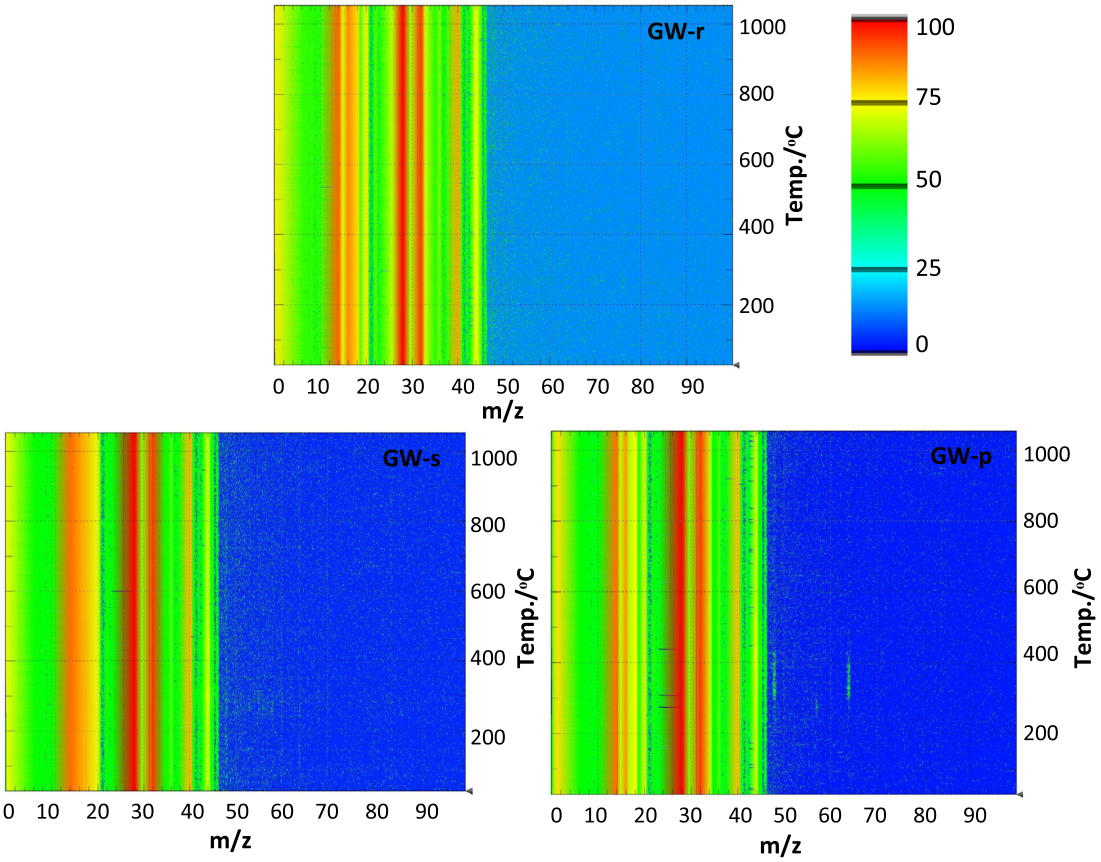

Fig. 2. MS results of the glass wools.

and after drying the wetted specimens for 3 days at room temperature) of the materials.

3. Results and discussion

3.1. Tg/DSC-MS

The TG/DSC results of the prepared samples are presented in Fig. 1. The TG/DSC curves of the samples showed that the mass loss of the GW-r (i.e., without the resin) was below 1 wt% at 1000 °C, while those of the GW-s and GW-p were 9 wt% and 8 wt%, respectively. However, the main proportion of mass loss occurred at about 500 °C for the GW-s and 540 °C for the GW-p. Above this temperature, the TG/DSC curves were relatively straight, presenting almost no mass loss. Hence, heat treatment from 200 °C to about 550 °C could be used to gradually remove resin in glass wool.

It is important to note that the mass losses above 200 °C were associated with two exothermic peaks on the DSC curves of the GW-s and GW-p; this can likely be ascribed to the heat released during the burning of the organic resin. An endothermic peak, attributed to the melting of the resin, was observed on the three samples between 650 °C and 700 °C [28]. The slight differences in the temperature at which endothermic melting occurred among the samples is likely an effect of the resin.

The MS results are presented in Fig. 2. The divergences between the graphs can be attributed to the compounds released from specific glass wools during heating, while some of the convergences are caused by the carrier gas (i.e., air) that was used during the heating.

It can be seen that most of the released compounds had an m/z of below 45, except for sample GW–p, for which some peaks of the released compounds reached m/z = 48, m/z = 57, and m/z = 64 in the temperature ranges of 350–440 °C, 250–300 °C, and 300–400 °C, respectively. The relative intensity of the mass spectra peaks of these released compounds remained relatively low but were still noticeable in the background.

Considering the release of water and carbon dioxide that occurs upon heating organic compounds, the MS curves were specifically investigated at m/z = 18 and m/z = 44 (Fig. 3). Indeed, according to the National Institute for Standards and Technology (NIST) Chemistry WebBook [29], when evaluating released compounds, m/z = 18 and m/z = 44 may be attributable to ionized water and carbon dioxide, respectively. The assignment of these m/z to specific compounds is not straightforward, however, as they could correspond to a single or to multiple ionized compounds. For instance, m/z = 44 could also be attributed to $C_2H_6N^+$, whereas m/z = 57 could be ascribed to a $C_4H_9^+$ molecule fragment [30].

The temperature at which these peaks appeared corresponded to the exothermic peaks in the DSC curves (Fig. 1) for m/z = 44, showing the combustion of the resin. However, they were different for the two resin-based samples, as a result of the different effect of each type of resin on the thermal behavior.

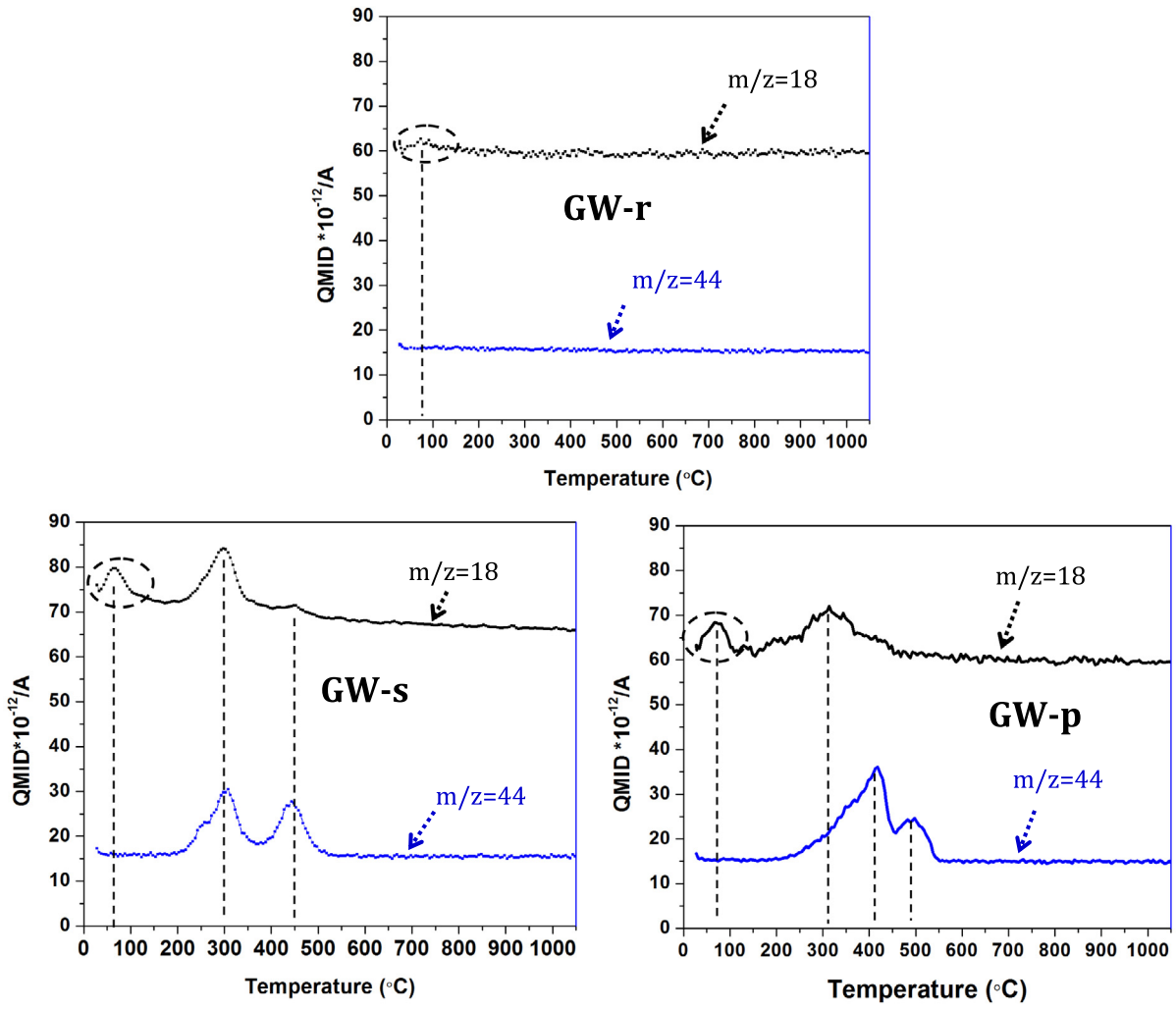

Fig. 3. MS curves of ionized compounds with m/z = 18 and m/z = 44.

Because the reference sample was free of resin, the curve for m/z = 18 and m/z = 44 was almost flat. However, a small inflection was observed on the m/z = 18 curve at around 100 °C, ascribed to the loss of adsorbed water. Another observation was the fact that the m/z = 18 curve was almost flat for the GW-p sample, likely suggesting a lower amount of structural water in the phenolic resin in comparison to the sugar resin. Although m/z = 17 and m/z = 28 were also checked in relation to ionized compounds, no relevant information was obtained; if they had been present, they could have been an indication of the presence of NH_3^+ and CO^+.

3.2. Milling efficiency

The particle size information is presented in Table 3. It was noticed that the milling efficiency of the wool was reduced due to the presence of organic resin; therefore, longer milling times were needed for samples containing the organic resin in order to achieve approximately the same particle size distribution as that in the reference sample. This could be due to the binding properties of the resin—the resin could agglomerate the glass wool particles together, decreasing the milling efficiency.

3.3. FTIR analysis

The FTIR spectra of the glass wool and prepared alkali-activated materials are presented in Fig. 4. The lower graphs (blue lines) are for the unreacted glass wool, while the upper graphs (red lines) are for the alkali-activated glass wool. The shoulder at around 3400 cm^{-1} can be ascribed to O-H stretching from the water [31]. This water is mainly adsorbed water in the case of unreacted glass wool, while it is structural and adsorbed water in the case of alkali-activated glass wools, where the shoulders were more pro-

Table 3
Particle size information for the milled wools.

	Particle size information				Density (g/cm^3)
Samples' milling time	Mean [μm]	d_{10} [μm]	Median (d_{50}) [μm]	d_{90} [μm]	
GW-r: 1 h	9.24	1.47	6.90	20.60	0.802
GW-s: 1 h	25.41	2.50	13.56	58.98	0.649
GW-p: 1 h	16.78	2.03	10.40	34.28	0.750
GW-s: 1 h 30 min	11.63	1.53	8.59	26.33	0.657
GW-p: 1 h 20 min	9.53	1.29	7.33	21.63	0.755

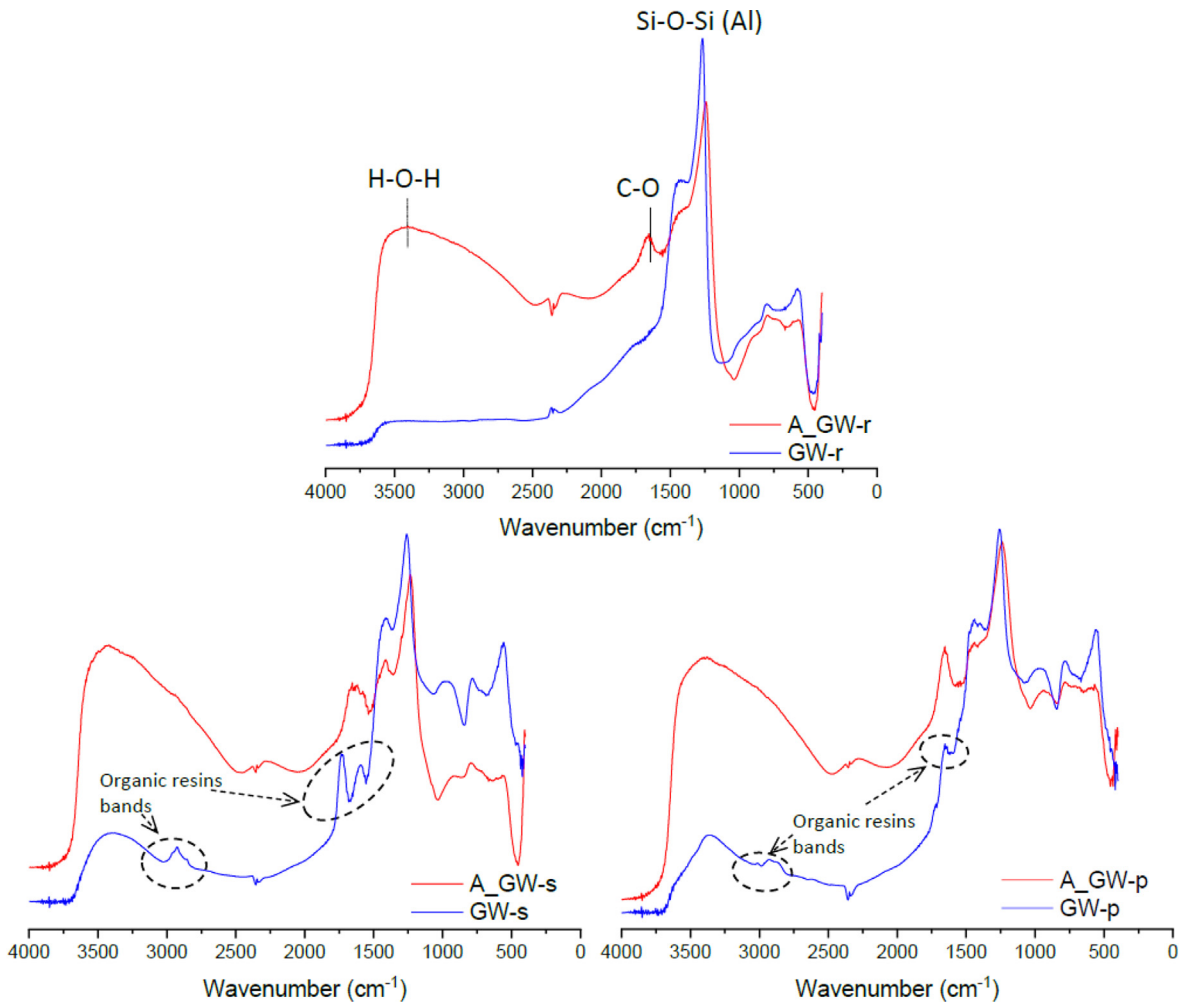

Fig. 4. The infrared (IR) patterns of the glass wools (GW-r, GW-s, and GW-p, shown in blue) and alkali-activated glass wools (A_GW-r, A_GW-s, and A_GW-p, shown in red). (For interpretation of the references to colour in this figure legend, the reader is referred to the web version of this article.)

nounced due to the higher water content. The bands at around 2850 cm^{-1} to 3000 cm^{-1} in the GW-s and GW-p are characteristic of an aliphatic C–H bond [32–34], resulting from the presence of organic resin. Consequently, this band was not present in the GW-r spectrum, due to the absence of organic resin in the reference glass wool. The band at around 1700 cm^{-1} to 1600 cm^{-1} can be attributed to the stretching vibration of C = O [35] in the organic resin—likely the carboxyl and aldehyde group in the GW-s and GW-p samples. Consequently, this band was absent in the GW-r. For the case of alkali-activated materials, the presence of this band likely resulted from the reaction of non-reacted sodium that had formed sodium carbonate in the presence of CO_2. The bands around 1400 cm^{-1} and 1260 cm^{-1} are attributable to carbonate vibration and Si-O/AlO stretching, respectively [36].

3.4. Calorimetry and rheology

Alkali activation is an exothermic reaction, and a calorimetry analysis can provide important information to help in differentiating between the precursors [37,38]. In this study, the isothermal calorimetry analysis was performed at temperatures of 20 °C, 40 °C, and 60 °C on alkali-activated materials prepared with the same A/P (0.75). The cumulative heat released (Fig. 5) was observed to increase with an increasing curing temperature for each of the three glass wools. However, the reference samples (A_GW-r) released more heat during the first 24 h at 20 °C, 40 °C, and 60 °C compared to the glass wools containing resin.

For comparative purposes, the cumulative heats released at 20 °C in the alkali-activated glass wools used for mechanical testing (prepared according to the mix design shown in Table 2) were also assessed (Fig. 5B) and were found to be comparable to those from the fresh mixtures prepared at the same temperature with an A/P of 0.75 (Fig. 5A). This indicated that increasing the A/P in the experimental studied range did not have a significant influence on the cumulative heat released. The cumulative heat released also increased with the curing temperature, with more heat being released at 60 °C (Fig. 5D) in comparison to 40 °C (Fig. 5C) and 20 °C (Fig. 5A). At higher temperatures, the slight reduction in the cumulative heat released, resulting from the presence of organic resin, was maintained and was more marked in samples containing sugar resin (A_GW-s).

The rheology study was performed at 20 °C on the alkali-activated materials prepared with the same L/S (0.80), and the results are presented in Fig. 6.

The alkali-activated glass wools were observed to present different rheological behaviors because of the effect of the organic resin. Although it presented a slightly finer particle size distribution (Table 1), the A_GW-r also presented the lowest liquid demand in the preparation of alkali-activated materials, resulting in a lower stress required for mixing the slurry when the A/P was the same for all the wools. It was noted that the A_GW-p required a higher shear stress in comparison to the A_GW-s, consistent with its higher liquid demand, observed in the preparation of the alkali-activated paste (Table 3). A higher A/P also means a

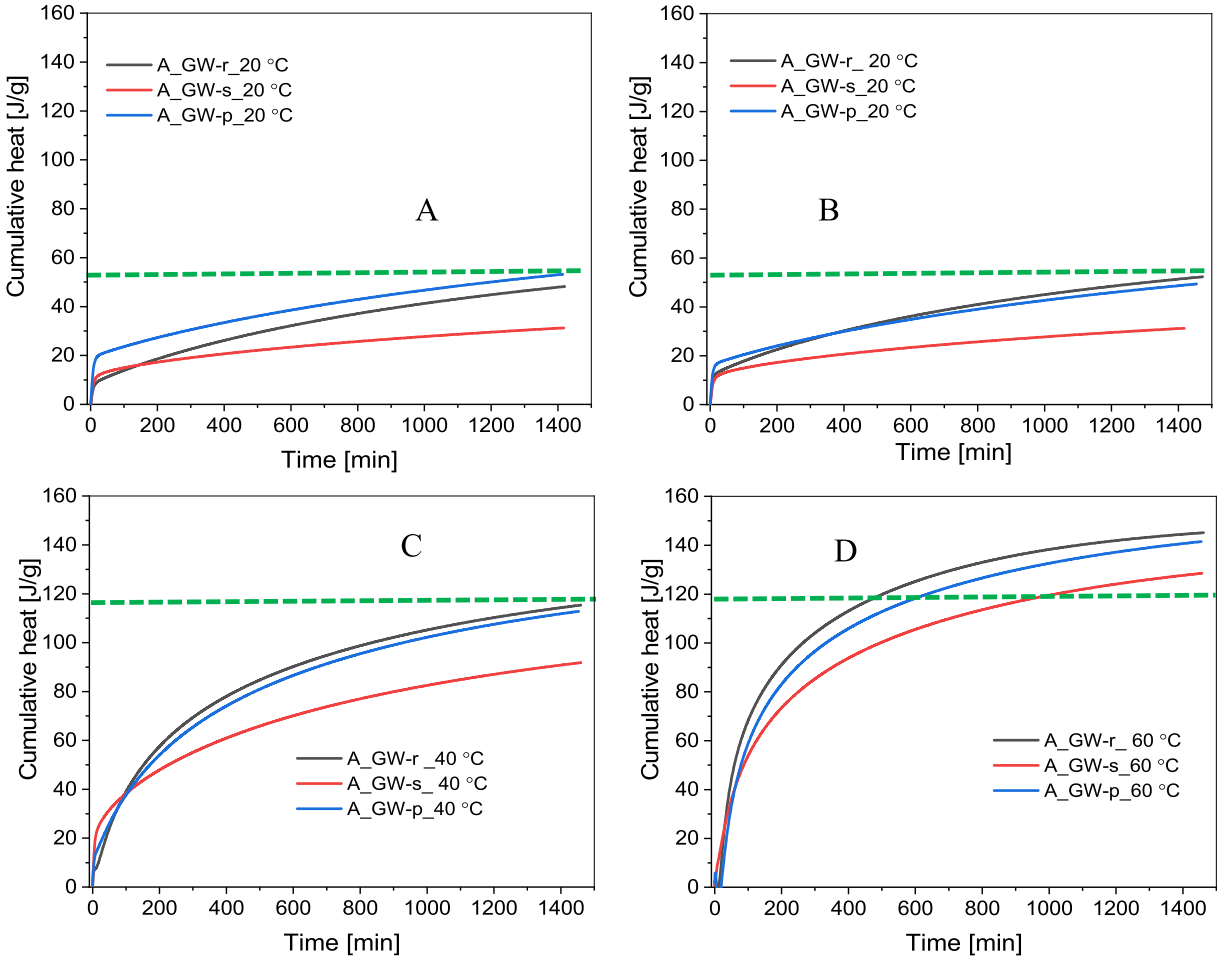

Fig. 5. Isothermal calorimetry curves of prepared alkali-activated glass wools (A) 20 °C, activator-to-precursor ratio (A/P) = 0.75; (B) 20 °C, A/P as in Table 2; (C) 40 °C, A/P = 0.75; and (D) 60 °C A/P = 0.75. The horizontal dashed lines are for the purpose of comparison.

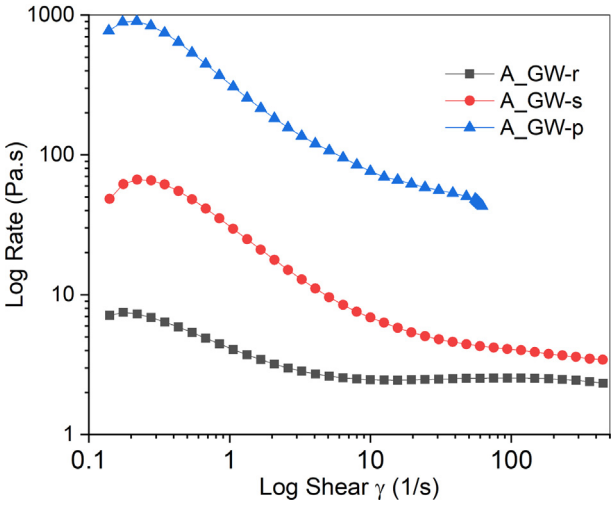

Fig. 6. Shear rate versus shear stress of the prepared geopolymer slurries.

higher water or alkaline-solution demand, with a related negative effect on the production cost, as the alkali activator is typically the most expensive raw material of the mix. Hence, based on the rheology results, the A_GW-s would be more economical in comparison to the A_GW-p in the production of alkali-activated materials.

3.5. Microstructural characterization

The microstructures of the as-received and milled GW-r, GW-s, and GW-p are presented in Fig. 7. From this figure, it can be observed that the glass wools were made of different fibers, with diameters varying from about 3 μm to 15 μm. Some spots that can be ascribed to the presence of the organic resin were also observed in the GW-s and GW-p. The scanning electron microscopy (SEM) images of the milled wool show that the milling was efficient. The milled wools had comparable appearances and contained some circular residual wool fibers with a maximum length around 40 μm.

The SEM images of the prepared materials from the glass wools are presented in Fig. 8. Some cracks can be observed on the microstructures of all the geopolymers. The presence of cracks can be attributed to the specimen preparation for SEM analysis, the high level of water loss due to elevated curing temperatures, and/or the exposure of the samples to a vacuum during the SEM process [5]. It should also be noted that the dissolution of the glass wool was not complete, as relics of glass wool fibers were still visible after alkali activation. The unreacted glass wool fibers in the A_GW-r appeared to be short and well incorporated in the matrix, which was slightly different from those observed in the A_GW-s and A_GW-p. This difference may be due to the absence of organic resin and to the slightly higher degree of fineness of the GW_r, indicated by its d_{50} values (Table 1); indeed, particle size is closely

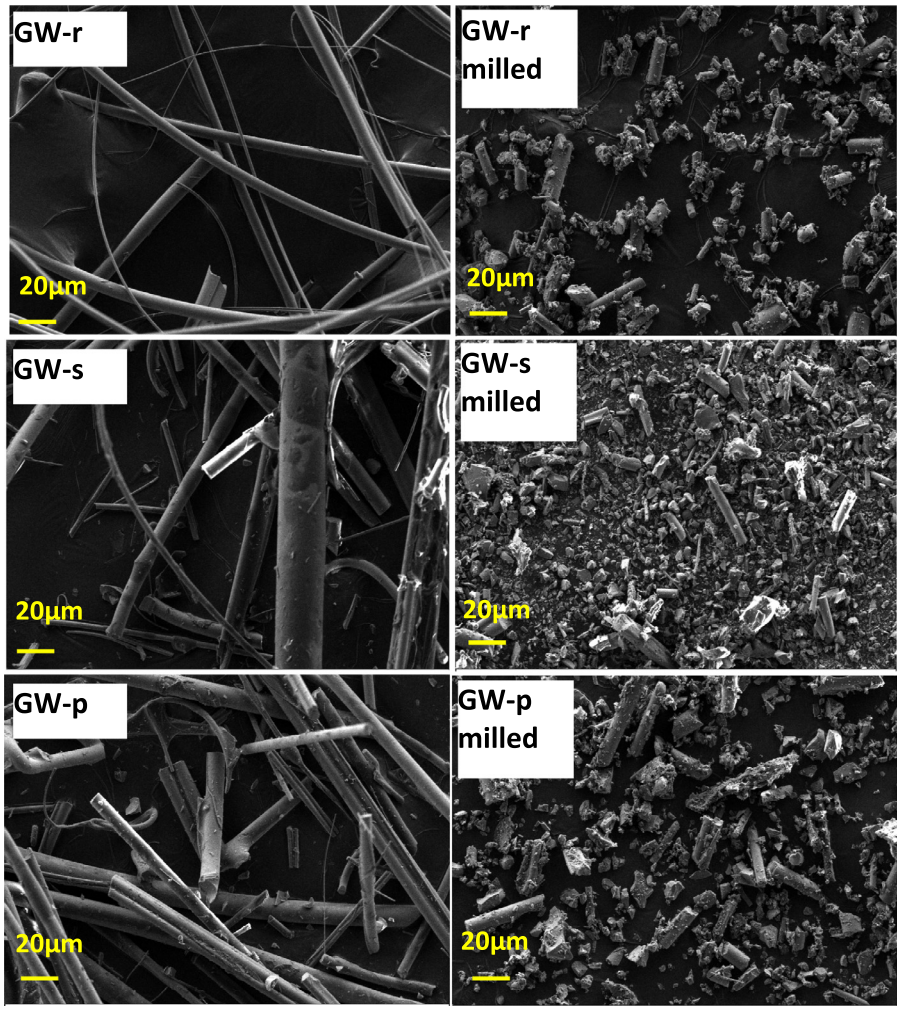

Fig. 7. Microstructural features of the as-received and milled GW-r, GW-s, and GW-p.

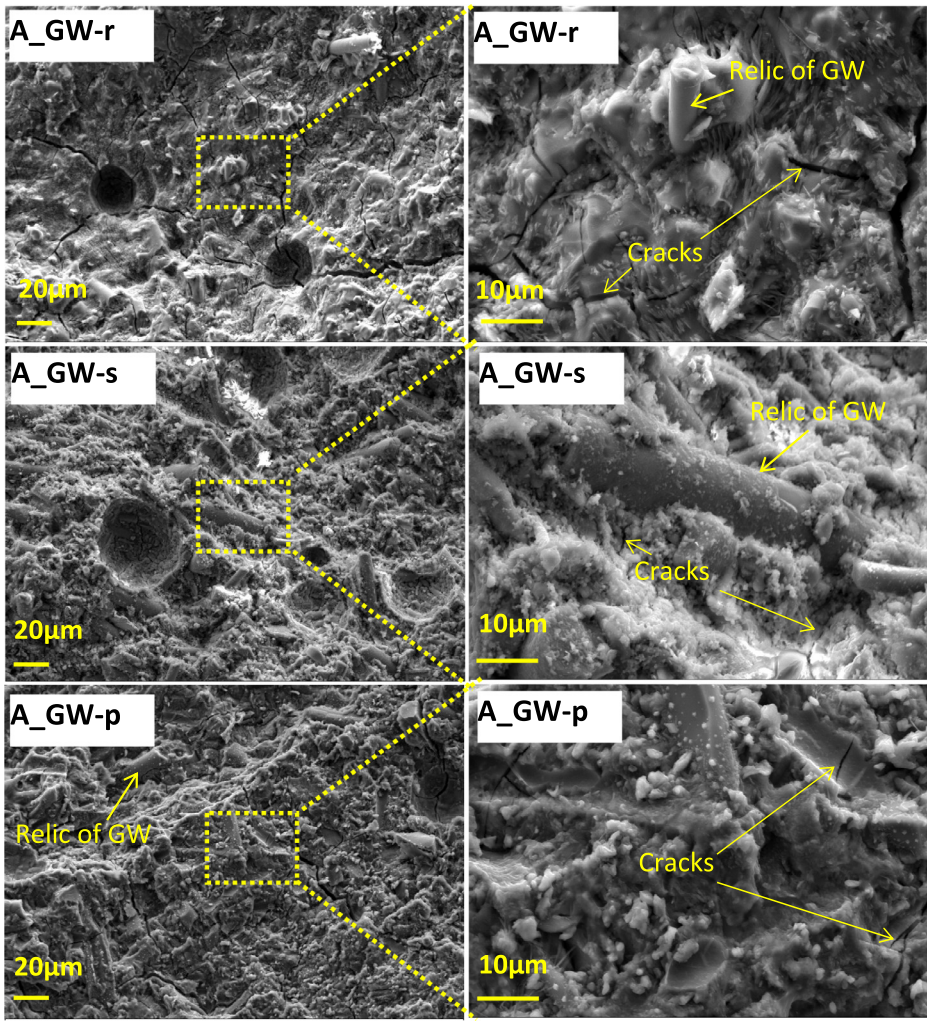

Fig. 8. Microstructural features of the prepared alkali-activated glass wools.

linked to higher surface area and, thus, to a higher reactivity of the material [39]. In the SEM results of the A_GW-s and A_GW-p, the surface of the residual glass wool fibers appeared to be less altered, likely due to the presence of the resin.

The results of the EDS analysis showed a closer gel composition for the A_GW-s and A_GW-p (Fig. 9). For the case of the A_GW-r, the dissolved phase was richer in Ca, suggesting that the organic resin affected the dissolution process of the glass wool. This may be correlated to the lower cumulative heat released in the specimens containing resin, as observed in Fig. 5. However, it is worth noting that the diffused Ca and Al present were not enough to contribute to the formation of a C-A-S-H gel, as evidenced in the Al_2O_3-SiO_2-CaO diagram from the A_GW-r and in previous studies [5,40].

3.6. XRD analysis

The XRD patterns of the glass wools and related alkali-activated materials (Fig. 10) revealed that the presence of organic resin had no effect on the XRD, as the main reaction products of the alkali-activated glass wool were X-ray amorphous. This is consistent with previous studies on alkali-activated glass wool, in which an amorphous sodium silicate gel was observed as the main reaction product upon its activation with a sodium silicate solution [5].

An observation of the curves, however, showed few nanocrystalline phases. This can be ascribed to the presence of stainless steel (Fe-Cr; powder diffraction file [PDF] 00–034-0396), likely from the grinding operation. This was more marked in resin-based samples because they spent more time in the grinding jar. A comparison of the amorphous hump of the glass wool and related alkali-activated materials showed a slight difference; the hump became slightly sharper for the alkali-activated materials, which is likely due to an increase in the structural order after alkali activation.

3.7. Compressive strength and water stability test

The results related to the compressive strength of the prepared alkali-activated materials at days 1, 3, and 28 at different curing temperatures are presented in Fig. 11. When curing at room temperature, the strength was observed to gradually increase with the curing time, varying from about 5 MPa at 1 day to 60 MPa at 28 days for the A_GW-r. Meanwhile, the compressive strength at 28 days was about 50 MPa and 45 MPa for the A_GW-p and A_GW-s, respectively. Hence, the presence of organic resin slightly reduced the strength development at room temperature; this is consistent with the cumulative heat release shown in Fig. 5.

The higher compressive strength achieved for all the samples at room temperature can likely be attributed to an increase in Si-O-Si bonds from the dissolved glass wool when activated with the alkaline solution [26]. For the samples that were first cured at 40 °C and

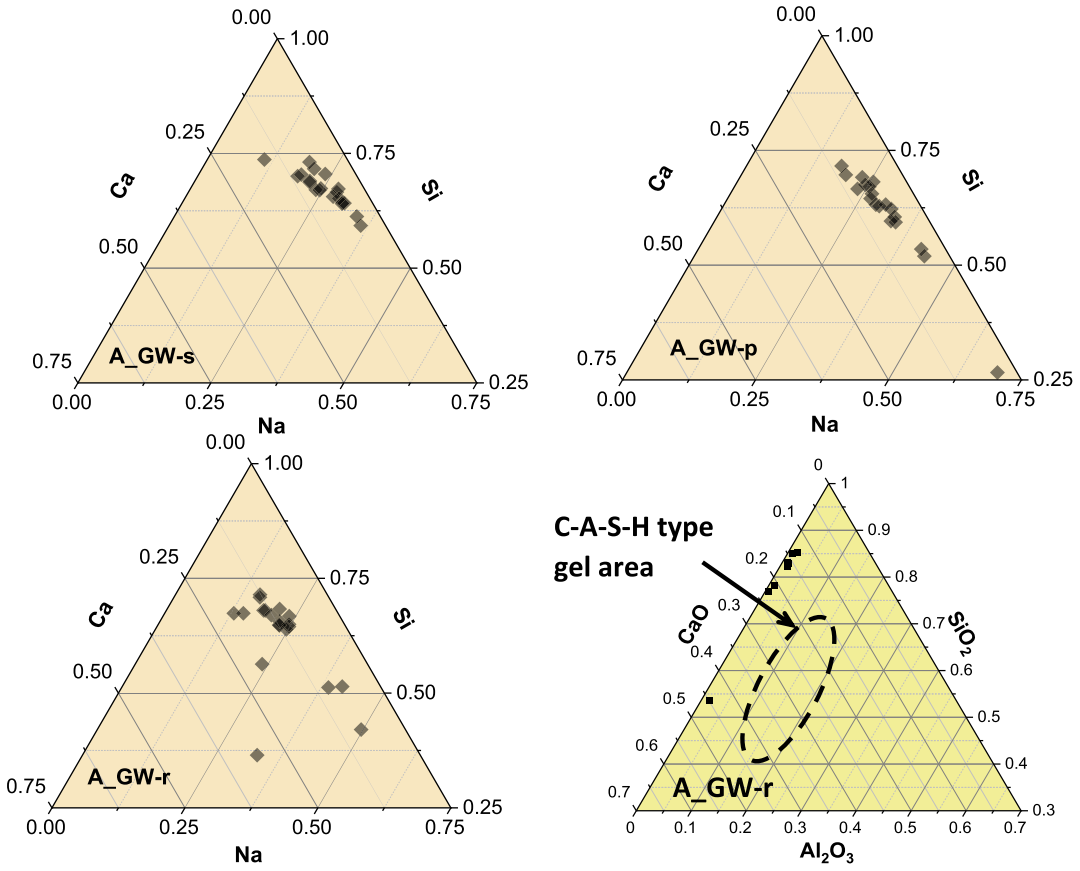

Fig. 9. Atomic EDS analysis of the prepared alkali-activated materials.

60 °C for 1 day before being moved to room temperature for the remaining curing period, no strength increase was observed between day 1 and day 3. The values of the strength were 25 MPa, 10 MPa, and 7 MPa for the A_GW-r, A_GW-p, and A_GW-s, respectively, after 1 day of curing at 40 °C. For the samples cured at 60 °C, the values of strength after 1 day were 16 MPa, 7 MPa, and 5 MPa for the A_GW-r, A_GW-p, and A_GW-s, respectively.

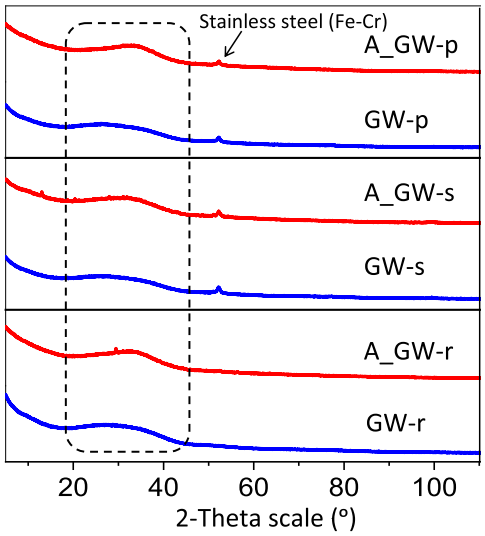

Fig. 10. XRD patterns of the prepared alkali-activated materials.

With the change of the curing temperature from 40/60 °C to room temperature (about 20 °C), the reaction kinetic decreased, in agreement with some previous studies on alkali-activated materials, demonstrating that curing above room temperature could accelerate the reaction kinetics of some geopolymer precursors [41,42]. Hence, for samples cured at 40/60 °C for 1 day, a higher extent of reaction was achieved that first day. When the samples were then moved to room temperature, no significant change in strength was observed during the next 2 days (i.e., at day 3 of curing); however, the reaction/hardening slowly evolved with time and led to greater strength at 28 days. For samples cured for the entire period at 20 °C, the strength increased much more gradually between day 1 and day 28. The strength of the A_GW-r sample slightly decreased between day 1 and day 3 when initially cured at 40 °C, in comparison to 60 °C. The exact reason for this decrease is not known and would require further research to determine.

Together, the A_GW-r, A_GW-s, and A_GW-p samples presented a high degree of similarity in terms of strength evolution when subjected to the 3 curing regimes, with no strength gain or lower strength values at 28 days for samples initially cured at 60 °C. The few differences observed can be attributed to the effect of the resins, which influenced the dissolution, diffusion, and hardening reactions in different ways. Consequently, 60 °C is likely above the threshold temperature that is beneficial for strength development. This is in agreement with some previous studies that have reported the existence of a threshold curing temperature above which the formation of geopolymer gel and the strength development are hindered [43,44].

Based on the dry strength results, all the prepared alkali-activated glass wool samples would be suitable for building applications, at least in dry environments, as the minimum requirement

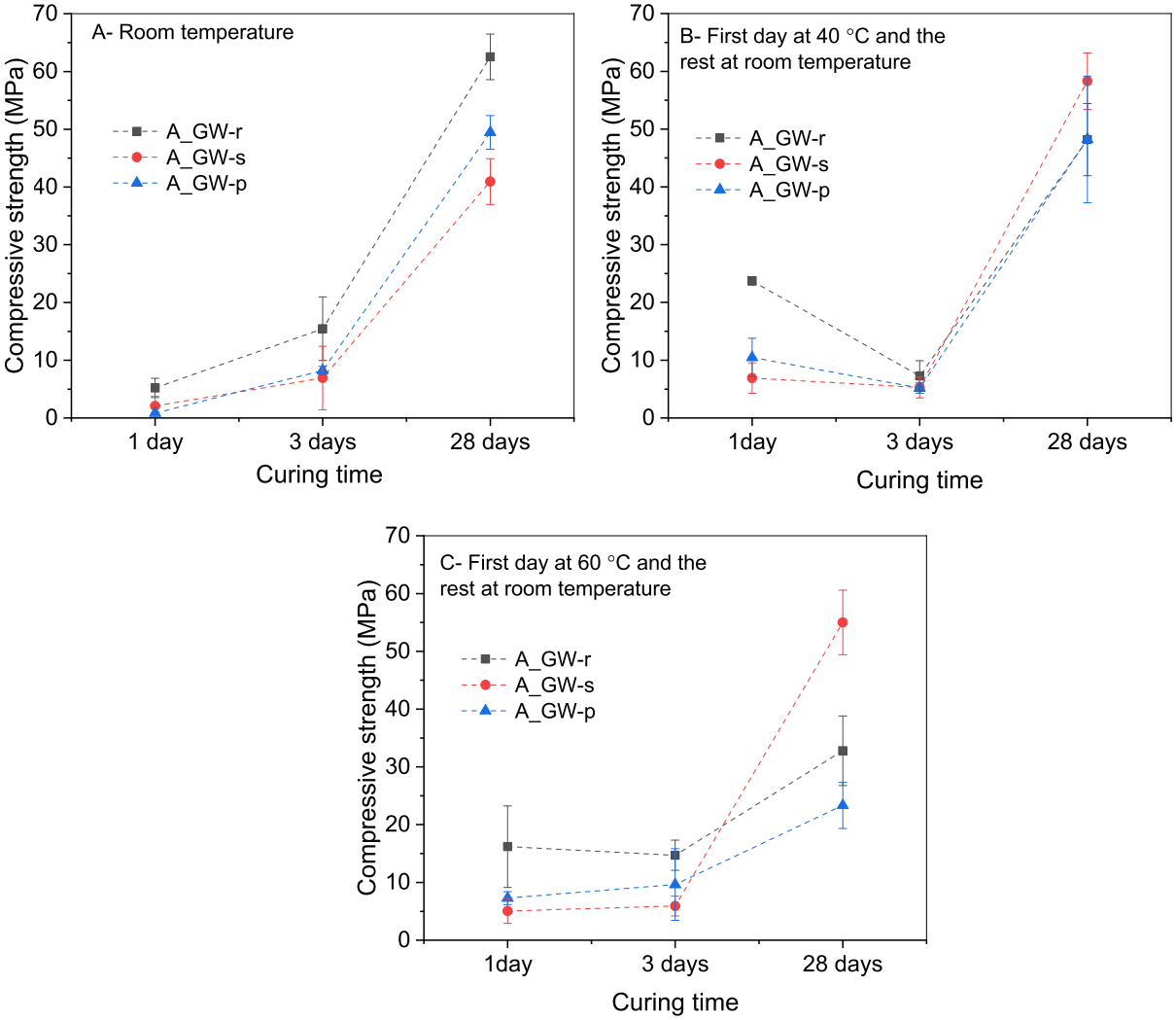

Fig. 11. The 1, 3 and 28-day compressive strength of activated materials during different curing regimes.

of compressive strength for many building applications—usually around 20 MPa—was met [45]. However, the stability in water of the prepared alkali-activated materials was also studied. The wet strength (i.e., after immersing in water for 24 h) and wet–dry strength (i.e., after immersing in water for 24 h and drying the wetted specimens for 3 days at room temperature) of the prepared alkali-activated materials are presented in Table 4.

It can be seen from Table 4 that the compressive strength decreased drastically after immersion in water. The wet and wet–dry strength values of the A_GW-p are not presented because the related samples were not stable in water (i.e., partial disintegration occurred). The decrease in strength was due to the poor hydrolytic stability of the binder gel. In a previous study that used a similar mix design and curing conditions, it was found that the binder gel consisted of Ca- and Al-poor sodium silicate gel [5]. This type of gel has low hydrolytic stability and dissolves in water [46,47]. However, the strength was partly recovered after the drying of the immersed samples. A similar behavior was observed in relation to the alkali activation of other geopolymer precursors—such as volcanic ashes and laterites—and was suggested to be associated with the hydration of some Si-O bonds, creating Si-OH and weakening the structure [48]. However, the product from the latter precursors was more stable, and the strength retention in a wet condition was higher (above 40%).

Another important observation was the difference in strength loss between the different alkali-activated glass wools. The presence of the organic resin negatively influenced the wet strength, mainly in the A_GW-p sample, for which partial disintegration was observed. Indeed, the high dry strength observed can be ascribed to the formation of amorphous sodium silicate gel—as identified in a study of the reaction mechanism of alkali-activated glass wool [5]—which is, however, water sensitive. Hence, the development of alkali-activated glass wool with improved water resistance properties would require the incorporation of more reactive geopolymer precursors such as metakaolin, stone wool, or ground granulated blast furnace slag (GGBS).

Table 4
Dry, wet, and wet–dry compressive strength of the A-GW-r, A-GW-s, and A-GW-p samples.

Sample name	Dry compressive strength (MPa)	Wet compressive strength (MPa)	Wet–dry compressive strength (MPa)
A-GW-r	60	22	25
A-GW-s	45	6	23
A-GW-p	50	Poor water stability	

4. Conclusions

This paper provided insight into the effect of organic resin on the properties of glass wool wastes and the resulting alkali-

activated materials. Three types of glass wool were used: the reference without the resin (GW-r), glass wool containing sugar-based resin (GW-s), and glass wool containing phenolic-based resin (GW-p). The results of this study lead to the following conclusions:

- The presence of organic resin reduced the milling efficiency of the glass wool, increased the liquid demand, and mitigated the development of compressive strength at room temperature and the water stability of the prepared materials.
- Curing for 24 h at 40 °C was beneficial for strength development at 1 day, in comparison to 20 °C and 60 °C, independent of the presence of resin. However, the effect of the presence of resin on the dry strength at day 28 was less obvious.
- The dry compressive strength values of all the prepared alkali-activated materials at day 28 were above 40 MPa, satisfying the requirement for their use as building materials in dry environments. The strength reduced after water immersion, and partial disintegration was observed in the GW-p-based alkali-activated materials.
- The microstructural study of the alkali-activated glass wool showed comparable features among the samples, with less obvious residual wool and a better diffusion of Ca in the binder system based on the GW-r, although this did not contribute to the formation of a C–A–S–H gel.
- The heat treatment of glass wool from 200 °C to about 550 °C could be applied to gradually remove the resin.

The current study confirmed the potential of valorizing glass wool waste for the production of building materials that are at least suitable for dry environments. A study of the effects of various co-binders on the properties and stability of alkali-activated materials containing these glass wools will be of interest in future.

Declaration of Competing Interest

The authors declare that they have no known competing financial interests or personal relationships that could have appeared to influence the work reported in this paper.

Acknowledgements

This work was performed in the framework of WOOL2LOOP H2020 project grant #821000. A substantial part of the experimental work was performed by Anne Heikkila in the framework of her master's thesis. Adeolu Adediran received funding from Auramo-säätiö for his doctoral research. Tero Luukkonen and Juho Yliniemi received funding from the Academy of Finland (grant #326291 and #322786, respectively). Part of the work was carried out with the support of the Centre for Material Analysis, University of Oulu, Finland. The authors thank Permakem AS for generously supplying the sodium silicate solution used in this investigation.

References

[1] C. Zhao, L.H. Mark, E. Chang, R.K.M. Chu, P.C. Lee, C.B. Park, Highly expanded, highly insulating polypropylene/polybutylene-terephthalate composite foams manufactured by nano-fibrillation technology, Materials & Design. 188 (2020) 108450, https://doi.org/10.1016/j.matdes.2019.108450.
[2] S. Deshmukh, H. Ronge, S. Ramamoorthy, Design of periodic foam structures for acoustic applications: Concept, parametric study and experimental validation, Materials & Design. 175 (2019) 107830, https://doi.org/10.1016/j.matdes.2019.107830.
[3] J. Yliniemi, T. Luukkonen, A. Kaiser, M. Illikainen, Mineral wool waste-based geopolymers, IOP Conference Series: Earth and Environmental Science. 297 (1) (2019) 012006, https://doi.org/10.1088/1755-1315/297/1/012006.
[4] A. Adediran, P.N. Lemougna, J. Yliniemi, P. Tanskanen, P. Kinnunen, J. Roning, M. Illikainen, Recycling glass wool as a fluxing agent in the production of clay- and waste-based ceramics, Journal of Cleaner Production. 289 (2021) 125673, https://doi.org/10.1016/j.jclepro.2020.125673.
[5] J. Yliniemi, B. Walkley, J.L. Provis, P. Kinnunen, M. Illikainen, Nanostructural evolution of alkali-activated mineral wools, Cement and Concrete Composites. 106 (2020) 103472, https://doi.org/10.1016/j.cemconcomp.2019.103472.
[6] J. Yliniemi, P. Kinnunen, P. Karinkanta, M. Illikainen, Utilization of Mineral Wools as Alkali-Activated Material Precursor, Materials. 9 (2016) 312.
[7] V. Karayannis, A. Moutsatsou, A. Domopoulou, E. Katsika, C. Drossou, A. Baklavaridis, Fired ceramics 100% from lignite fly ash and waste glass cullet mixtures, Journal of Building, Engineering. 14 (2017) 1–6, https://doi.org/10.1016/j.jobe.2017.09.006.
[8] J.F. Rivera, Z.I. Cuarán-Cuarán, N. Vanegas-Bonilla, R. Mejía de Gutiérrez, Novel use of waste glass powder: Production of geopolymeric tiles, Advanced Powder Technology. 29 (12) (2018) 3448–3454, https://doi.org/10.1016/j.apt.2018.09.023.
[9] A. Shayan, A. Xu, Value-added utilisation of waste glass in concrete, Cement and Concrete Research. 34 (1) (2004) 81–89, https://doi.org/10.1016/S0008-8846(03)00251-5.
[10] P. Guo, W. Meng, H. Nassif, H. Gou, Y.i. Bao, New perspectives on recycling waste glass in manufacturing concrete for sustainable civil infrastructure, Construction and Building Materials. 257 (2020) 119579, https://doi.org/10.1016/j.conbuildmat.2020.119579.
[11] M.N.N. Khan, A.K. Saha, P.K. Sarker, Reuse of waste glass as a supplementary binder and aggregate for sustainable cement-based construction materials: A review, Journal of Building Engineering. 28 (2020) 101052, https://doi.org/10.1016/j.jobe.2019.101052.
[12] S. Luhar, T.-W. Cheng, D. Nicolaides, I. Luhar, D. Panias, K. Sakkas, Valorisation of glass wastes for the development of geopolymer composites – Durability, thermal and microstructural properties: A review, Construction and Building Materials. 222 (2019) 673–687, https://doi.org/10.1016/j.conbuildmat.2019.06.169.
[13] H. Nguyen, A. Kaas, P. Kinnunen, V. Carvelli, C. Monticelli, J. Yliniemi, M. Illikainen, Fiber reinforced alkali-activated stone wool composites fabricated by hot-pressing technique, Materials & Design. 186 (2020) 108315.
[14] R.D. Rawlings, J.P. Wu, A.R. Boccaccini, Glass-ceramics: their production from wastes—a review, Journal of Materials Science. 41 (2006) 733–761.
[15] E. Furlani, G. Tonello, S. Maschio, Recycling of steel slag and glass cullet from energy saving lamps by fast firing production of ceramics, Waste Management. 30 (8-9) (2010) 1714–1719, https://doi.org/10.1016/j.wasman.2010.03.030.
[16] L. Mao, H. Zhou, M. Peng, L. Hu, W. Zhang, Effects of waste glass particle size on improving the property and environmental safety of fired brick containing electroplating sludge, Construction and Building Materials. 257 (2020) 119583, https://doi.org/10.1016/j.conbuildmat.2020.119583.
[17] A. Zimmer, S.R. Bragança, A review of waste glass as a raw material for whitewares, Journal of Environmental Management. 244 (2019) 161–171, https://doi.org/10.1016/j.jenvman.2019.05.038.
[18] N. Phonphuak, S. Kanyakam, P. Chindaprasirt, Utilization of waste glass to enhance physical–mechanical properties of fired clay brick, Journal of Cleaner Production. 112 (2016) 3057–3062, https://doi.org/10.1016/j.jclepro.2015.10.084.
[19] M.U. Rehman, M. Ahmad, K. Rashid, Influence of fluxing oxides from waste on the production and physico-mechanical properties of fired clay brick: A review, Journal of Building Engineering. 27 (2020) 100965, https://doi.org/10.1016/j.jobe.2019.100965.
[20] J. Yliniemi, O. Laitinen, P. Kinnunen, M. Illikainen, Pulverization of fibrous mineral wool waste, Journal of Material Cycles and Waste, Management. 20 (2) (2018) 1248–1256.
[21] T. Kovářík, J. Hájek, M. Pola, D. Rieger, M. Svoboda, J. Beneš, P. Šutta, K. Deshmukh, V. Jandová, Cellular ceramic foam derived from potassium-based geopolymer composite: Thermal, mechanical and structural properties, Materials & Design. 198 (2021) 109355, https://doi.org/10.1016/j.matdes.2020.109355.
[22] M. Chougan, S.H. Ghaffar, P. Sikora, S.-Y. Chung, T. Rucinska, D. Stephan, A. Albar, M.R. Swash, Investigation of additive incorporation on rheological, microstructural and mechanical properties of 3D printable alkali-activated materials, Materials & Design. 202 (2021) 109574, https://doi.org/10.1016/j.matdes.2021.109574.
[23] M. Lahoti, K.K. Wong, K.H. Tan, E.-H. Yang, Effect of alkali cation type on strength endurance of fly ash geopolymers subject to high temperature exposure, Materials & Design. 154 (2018) 8–19, https://doi.org/10.1016/j.matdes.2018.05.023.
[24] Z. Li, I. Alfredo Flores Beltran, Y. Chen, B. Šavija, G. Ye, Early-age properties of alkali-activated slag and glass wool paste, Construction and Building Materials. 291 (2021) 123326, https://doi.org/10.1016/j.conbuildmat.2021.123326.
[25] M. Mastali, A. Zahra, K. Hugo, R. Faraz, Utilization of mineral wools in production of alkali activated materials, Construction and Building Materials. 283 (2021) 122790, https://doi.org/10.1016/j.conbuildmat.2021.122790.
[26] M. Pavlin, B. Horvat, A. Frankovič, V. Ducman, Mechanical, microstructural and mineralogical evaluation of alkali-activated waste glass and stone wool, Ceramics International. 47 (11) (2021) 15102–15113, https://doi.org/10.1016/j.ceramint.2021.02.068.
[27] EN 196-1, Methods of testing cement. Determination of strength, 2016.
[28] P.N. Lemougna, J. Yliniemi, A. Adediran, T. Luukkonen, P. Tanskanen, M. Finnilä, M. Illikainen, Synthesis and characterization of porous ceramics from spodumene tailings and waste glass wool, Ceramics International. 47 (23) (2021) 33286–33297, https://doi.org/10.1016/j.ceramint.2021.08.231.

[29] NIST, NIST Chemistry WebBook (https://webbook.nist.gov/), (2018). https://webbook.nist.gov/.
[30] A. Zafar, J. Schjødt-Thomsen, R. Sodhi, R. Goacher, D. de Kubber, Investigation of the ageing effects on phenol-urea-formaldehyde binder and alkanol amine-acid anhydride binder coated mineral fibres, Polymer Degradation and Stability. 98 (1) (2013) 339–347, https://doi.org/10.1016/j.polymdegradstab.2012.09.007.
[31] M. Criado, I. Sobrados, J. Sanz, Polymerization of hybrid organic–inorganic materials from several silicon compounds followed by TGA/DTA, FTIR and NMR techniques, Progress in Organic Coatings. 77 (4) (2014) 880–891, https://doi.org/10.1016/j.porgcoat.2014.01.019.
[32] C. Coury, A.M. Dillner, A method to quantify organic functional groups and inorganic compounds in ambient aerosols using attenuated total reflectance FTIR spectroscopy and multivariate chemometric techniques, Atmospheric Environment. 42 (23) (2008) 5923–5932, https://doi.org/10.1016/j.atmosenv.2008.03.026.
[33] M. Asemani, A.R. Rabbani, Detailed FTIR spectroscopy characterization of crude oil extracted asphaltenes: Curve resolve of overlapping bands, Journal of Petroleum Science and Engineering. 185 (2020) 106618, https://doi.org/10.1016/j.petrol.2019.106618.
[34] C. Peltre, E.G. Gregorich, S. Bruun, L.S. Jensen, J. Magid, Repeated application of organic waste affects soil organic matter composition: Evidence from thermal analysis, FTIR-PAS, amino sugars and lignin biomarkers, Soil Biology and Biochemistry. 104 (2017) 117–127, https://doi.org/10.1016/j.soilbio.2016.10.016.
[35] S. Lin, Z. Liu, E. Zhao, J. Qian, X. Li, Q. Zhang, M. Ali, A study on the FTIR spectra of pre- and post-explosion coal dust to evaluate the effect of functional groups on dust explosion, Process Safety and Environmental Protection. 130 (2019) 48–56, https://doi.org/10.1016/j.psep.2019.07.018.
[36] P. Perumal, H. Niu, J. Kiventerä, P. Kinnunen, M. Illikainen, Upcycling of mechanically treated silicate mine tailings as alkali activated binders, Minerals Engineering. 158 (2020) 106587, https://doi.org/10.1016/j.mineng.2020.106587.
[37] H. Rahier, J. Wastiels, M. Biesemans, R. Willlem, G. Van Assche, B. Van Mele, Reaction mechanism, kinetics and high temperature transformations of geopolymers, Journal of Materials Science. 42 (9) (2007) 2982–2996, https://doi.org/10.1007/s10853-006-0568-8.
[38] J.L. Provis, S.A. Bernal, Geopolymers and Related Alkali-Activated Materials, Annual Review of Materials Research. 44 (1) (2014) 299–327, https://doi.org/10.1146/matsci.2014.44.issue-110.1146/annurev-matsci-070813-113515.
[39] H. Niu, P. Kinnunen, H. Sreenivasan, E. Adesanya, M. Illikainen, Structural collapse in phlogopite mica-rich mine tailings induced by mechanochemical treatment and implications to alkali activation potential, Minerals Engineering. 151 (2020) 106331, https://doi.org/10.1016/j.mineng.2020.106331.
[40] P.N. Lemougna, A. Adediran, J. Yliniemi, A. Ismailov, E. Levanen, P. Tanskanen, P. Kinnunen, J. Roning, M. Illikainen, Thermal stability of one-part metakaolin geopolymer composites containing high volume of spodumene tailings and glass wool, Cement and Concrete Composites. 114 (2020) 103792, https://doi.org/10.1016/j.cemconcomp.2020.103792.
[41] Y. Zhang, R. Xiao, X. Jiang, W. Li, X. Zhu, B. Huang, Effect of particle size and curing temperature on mechanical and microstructural properties of waste glass-slag-based and waste glass-fly ash-based geopolymers, Journal of Cleaner Production. 273 (2020) 122970, https://doi.org/10.1016/j.jclepro.2020.122970.
[42] P. Zhang, K. Wang, Q. Li, J. Wang, Y. Ling, Fabrication and engineering properties of concretes based on geopolymers/alkali-activated binders - A review, Journal of Cleaner Production. 258 (2020) 120896, https://doi.org/10.1016/j.jclepro.2020.120896.
[43] X. Tian, W. Xu, S. Song, F. Rao, L. Xia, Effects of curing temperature on the compressive strength and microstructure of copper tailing-based geopolymers, Chemosphere. 253 (2020) 126754, https://doi.org/10.1016/j.chemosphere.2020.126754.
[44] P. Rovnaník, Effect of curing temperature on the development of hard structure of metakaolin-based geopolymer, Construction and Building Materials. 24 (7) (2010) 1176–1183, https://doi.org/10.1016/j.conbuildmat.2009.12.023.
[45] R. Taurino, A. Karamanov, R. Rosa, E. Karamanova, L. Barbieri, S. Atanasova-Vladimirova, G. Avdeev, C. Leonelli, New ceramic materials from MSWI bottom ash obtained by an innovative microwave-assisted sintering process, Journal of the European Ceramic Society. 37 (1) (2017) 323–331, https://doi.org/10.1016/j.jeurceramsoc.2016.08.011.
[46] P. Ana Balaguer, M.T. Tognonvi, T.-H. Arezki, WASTE GLASS POWDER-BASED ALKALI-ACTIVATED MORTAR, International Journal of Research, Engineering and Technology. 3 (2014) 15–19.
[47] R. Redden, N. Neithalath, Microstructure, strength, and moisture stability of alkali activated glass powder-based binders, Cement and Concrete Composites. 45 (2014) 46–56, https://doi.org/10.1016/j.cemconcomp.2013.09.011.
[48] P.N. Lemougna, U.F. Chinje Melo, M.-P. Delplancke, H. Rahier, Influence of the activating solution composition on the stability and thermo-mechanical properties of inorganic polymers (geopolymers) from volcanic ash, Construction and Building Materials. 48 (2013) 278–286, https://doi.org/10.1016/j.conbuildmat.2013.06.089.